
Out of the Shadows: Exploring a Latent Space for Neural Network Verification

Lukas Koller¹

Tobias Ladner¹

Matthias Althoff¹

¹Technical University of Munich
lukas.koller@tum.de

Abstract

Neural networks are ubiquitous. However, they are often sensitive to small input changes. Hence, to prevent unexpected behavior in safety-critical applications, their formal verification – a notoriously hard problem – is necessary. Many state-of-the-art verification algorithms use reachability analysis or abstract interpretation to enclose the set of possible outputs of a neural network. Often, the verification is inconclusive due to the conservatism of the enclosure. To address this problem, we design a novel latent space for formal verification that enables the transfer of output specifications to the input space for an iterative specification-driven input refinement, i.e., we iteratively reduce the set of possible inputs to only enclose the unsafe ones. The latent space is constructed from a novel view of projection-based set representations, e.g., zonotopes, which are commonly used in reachability analysis of neural networks. A projection-based set representation is a "shadow" of a higher-dimensional set – a latent space – that does not change during a set propagation through a neural network. Hence, the input set and the output enclosure are "shadows" of the same latent space that we can use to transfer constraints. We present an efficient verification tool for neural networks that uses our iterative refinement to significantly reduce the number of subproblems in a branch-and-bound procedure. Using zonotopes as a set representation, unlike many other state-of-the-art approaches, our approach can be realized by only using matrix operations, which enables a significant speed-up through efficient GPU acceleration. We demonstrate that our tool achieves competitive performance, which would place it among the top-ranking tools of the last neural network verification competition (VNN-COMP'24).

1 Introduction

Neural networks perform exceptionally well across many complex tasks, e.g., object detection [42] or protein structure prediction [21]. However, neural networks can be sensitive towards small input changes, e.g., often adversarial attacks can provoke misclassifications [17]. Thus, neural networks must be formally verified to avoid unexpected behavior in safety-critical applications, e.g., autonomous driving [11] or airborne collision avoidance [19], where the inputs can be influenced by sensor noise or external disturbances.

The goal of formal verification of neural networks is to find a mathematical proof that every possible output for a given input set is safe with respect to a given specification; in this work, we demand that the output avoids an unsafe set. The verification problem is undecidable in the general case [20] and NP-hard for neural networks with ReLU-activation functions [22]. Many prominent verification algorithms use reachability analysis or abstract interpretation to enclose the intersection of an unsafe set with the output of the neural network [15, 34, 39, 4, 25]: The input set is represented using a

continuous set representation (such as intervals or zonotopes), which is conservatively propagated through the layers of a neural network to enclose all possible outputs. If the intersection of the output enclosure with an unsafe set is empty, the safety of the given input set is formally verified. Out of the box, most reachability-based algorithms do not scale well to large neural networks with high-dimensional input spaces because the conservatism of the set propagation increases due to over-approximating nonlinearities in the neural network. Most verification algorithms reduce the conservatism by integrating a branch-and-bound procedure to recursively split the verification problem into smaller and simpler subproblems, e.g., by exploiting the piecewise linearity of a ReLU-activation function to reduce approximation errors [9] or splitting the input set to reduce its size. However, in the worst case, the verification problem is split into exponentially many subproblems, all of which must be verified.

In this paper, we speed up the formal verification of neural networks by iteratively refining the input set to only enclose the unsafe inputs. Thereby, we reduce the size of the input set to reduce the number of splits and, ultimately, the number of subproblems to be verified. For our iterative input refinement, we construct a novel latent space to transfer the unsafe set backwards through the network from the output space to the input space for the enclosure of all unsafe inputs, i.e., we can discard all inputs that are already proven to be safe. We construct the latent space by using projection-based set representations that represent the projection ("shadow") of a higher-dimensional set, e.g., a zonotope is the "shadow" of a higher-dimensional hypercube. The set propagation through a neural network only changes the "shadow", while the higher-dimensional set remains unchanged. Hence, all considered sets are different "shadows" of the same higher-dimensional set, representing a latent space. We can exploit the dependencies between the considered sets through our novel latent space to transfer the unsafe set from the output space to the input space to refine the input set [24]. Moreover, if we cannot verify the safety of the neural network, we can utilize the latent space to extract candidates for counterexamples. Ultimately, we propose a verification algorithm that integrates our novel iterative input refinement into a branch-and-bound procedure for verifying and falsifying neural networks. Unlike many other state-of-the-art verification algorithms, we implement our verification algorithm using only matrix operations to take full advantage of GPU acceleration to simultaneously verify entire batches of subproblems.

To summarize, our main contributions are:

- A latent space for the verification of neural networks constructed from a novel view of the propagation of projection-based sets where all considered sets are "shadows" of the same higher-dimensional set.
- By utilizing the latent space, we propose iterative specification-driven input refinement and an approach for counterexample extraction to speed up branch-and-bound verification and falsification of neural networks.
- An efficient algorithm that only uses matrix operations to take full advantage of GPU acceleration.
- An extensive evaluation and comparison with state-of-the-art neural network verification algorithms on benchmarks from the neural network verification competition 2024 (VNN-COMP'24) [8]. Additionally, we conduct extensive ablation studies to justify the design choices of our verification algorithm.

2 Preliminaries

2.1 Notation

Lowercase letters denote vectors and uppercase letters denote matrices. We denote the i -th entry of a vector x by $x_{(i)}$ and the entry in the i -th row and the j -th column of a matrix $A \in \mathbb{R}^{n \times m}$ by $A_{(i,j)}$. The i -th row is written as $A_{(i, \cdot)}$ and the j -th column as $A_{(\cdot, j)}$. The identity matrix is denoted by $I_n \in \mathbb{R}^{n \times n}$. We write the matrix (with appropriate size) that contains only zeros or ones as $\mathbf{0}$ and $\mathbf{1}$. Given two matrices $A \in \mathbb{R}^{m \times n_1}$ and $B \in \mathbb{R}^{m \times n_2}$, their (horizontal) concatenation is denoted by $[A \ B] \in \mathbb{R}^{m \times (n_1+n_2)}$. The operation $\text{Diag}(v)$ returns a diagonal matrix with the entries of vector v on its diagonal and the operation $|A|$ takes the elementwise absolute value of a matrix $A \in \mathbb{R}^{n \times m}$. We denote sets by uppercase calligraphic letters. Given two sets $\mathcal{S}_1, \mathcal{S}_2 \subset \mathbb{R}^n$, we write their Minkowski sum as $\mathcal{S}_1 \oplus \mathcal{S}_2 = \{s_1 + s_2 \mid s_1 \in \mathcal{S}_1, s_2 \in \mathcal{S}_2\}$. For $n \in \mathbb{N}$, $[n] = \{1, 2, \dots, n\}$ is the set of all

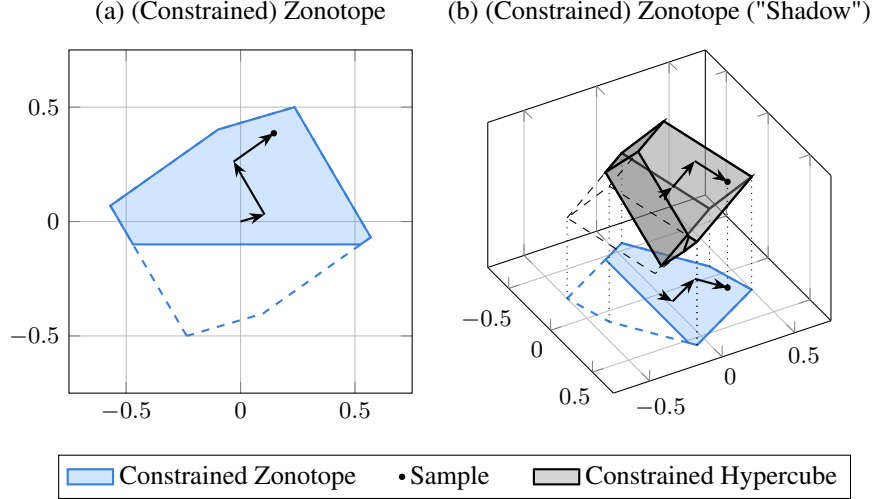


Figure 1: (a) An illustration of a constrained zonotope and a sample with its generators; (b) the same constrained zonotope as the "shadow" of a constrained hypercube.

natural numbers up to n . The n -dimensional interval $\mathcal{I} \subset \mathbb{R}^n$ with bounds $l, u \in \mathbb{R}^n$ is written as $\mathcal{I} = [l, u]$, where $\forall i \in [n]: l_{(i)} \leq u_{(i)}$. For a function $f: \mathbb{R}^n \rightarrow \mathbb{R}^m$, we abbreviate the image of $\mathcal{S} \subset \mathbb{R}^n$ with $f(\mathcal{S}) = \{f(s) \mid s \in \mathcal{S}\}$.

2.2 Feed-Forward Neural Networks

A (feed-forward) neural network $\Phi: \mathbb{R}^{n_0} \rightarrow \mathbb{R}^{n_\kappa}$ is a sequence of $\kappa \in \mathbb{N}$ layers. Each layer applies an affine map (linear layer) or an element-wise nonlinear activation function (nonlinear layer).

Definition 1 (Neural Network, [6, Sec. 5.1]). *For an input $x \in \mathbb{R}^{n_0}$, the output of a neural network $y = \Phi(x) \in \mathbb{R}^{n_\kappa}$ is*

$$h_0 = x, \quad h_k = L_k(h_{k-1}) \quad \text{for } k \in [\kappa], \quad y = h_\kappa,$$

where

$$L_k(h_{k-1}) = \begin{cases} W_k h_{k-1} + b_k & \text{if } k\text{-th layer is linear,} \\ \phi_k(h_{k-1}) & \text{otherwise,} \end{cases}$$

with weights $W_k \in \mathbb{R}^{n_k \times n_{k-1}}$, bias $b_k \in \mathbb{R}^{n_k}$, and nonlinear function ϕ_k that is applied element-wise.

2.3 Set-Based Computing

A zonotope is a convex set representation that is popular in reachability analysis due to its favorable computational complexity [35, 25].

Definition 2 (Zonotope, [16, Def. 1]). *Given a center $c \in \mathbb{R}^n$ and a generator matrix $G \in \mathbb{R}^{n \times q}$, a zonotope is defined as*

$$\mathcal{Z} = \langle c, G \rangle_{\mathcal{Z}} := \left\{ c + \sum_{i=1}^q G_{(\cdot, i)} \beta_{(i)} \mid \beta \in [-1, 1] \right\}.$$

Subsequently, we define the set-based operations for zonotopes required for our verification algorithm. The Minkowski sum of a zonotope $\mathcal{Z} = \langle c, G \rangle_{\mathcal{Z}} \subset \mathbb{R}^n$ and an interval $[\underline{x}, \bar{x}] \subset \mathbb{R}^n$ is computed by [2, Prop. 2.1 & Sec. 2.4]

$$\mathcal{Z} \oplus [\underline{x}, \bar{x}] = \langle c + 1/2(\bar{x} + \underline{x}), [G \text{ diag}(1/2(\bar{x} - \underline{x}))] \rangle_{\mathcal{Z}}. \quad (1)$$

The image of a zonotope $\mathcal{Z} = \langle c, G \rangle_{\mathcal{Z}} \subset \mathbb{R}^n$ under an affine map $f: \mathbb{R}^n \rightarrow \mathbb{R}^m$, $x \mapsto Wx + b$ with $W \in \mathbb{R}^{m \times n}$ and $b \in \mathbb{R}^m$ is computed by [2, Sec. 2.4]

$$f(\mathcal{Z}) = W\mathcal{Z} \oplus b = \langle Wc + b, WG \rangle_{\mathcal{Z}}. \quad (2)$$

Using an affine map, we can write a zonotope $\mathcal{Z} = \langle c, G \rangle_Z \subset \mathbb{R}^n$ with q generators, i.e., $G \in \mathbb{R}^{n \times q}$, as the projection of a q -dimensional (unit)-hypercube $\mathcal{B}_q = [-\mathbf{1}, \mathbf{1}]$: $\mathcal{Z} = c \oplus G \mathcal{B}_q$. Thus, intuitively, a zonotope is the "shadow" of a higher-dimensional hypercube.

A convex polytope is the intersection of a finite number of halfspaces [2, Def. 2.1]; we denote a polytope by $\langle A, b \rangle_H = \{x \in \mathbb{R}^n \mid Ax \leq b\} \subset \mathbb{R}^n$, where $A \in \mathbb{R}^{n \times p}$ and $b \in \mathbb{R}^p$.

All zonotopes are convex and point-symmetric. However, by constraining the hypercube, we can represent arbitrary convex polytopes [33, Thm. 1].

Definition 3 (Constrained Zonotope, [33, Def. 3]). *Given a zonotope $\mathcal{Z} = \langle c, G \rangle_Z \subset \mathbb{R}^n$ with $c \in \mathbb{R}^n$ and $G \in \mathbb{R}^{n \times q}$, the zonotope with constraints $C\beta \leq d$, for $\beta \in \mathcal{B}_q$ with $C \in \mathbb{R}^{p \times q}$ and $d \in \mathbb{R}^p$, is defined as*

$$\mathcal{Z}|_{C\beta \leq d} := \{c + G\beta \mid \beta \in [-\mathbf{1}, \mathbf{1}], C\beta \leq d\} = c \oplus G \overline{\mathcal{B}_q},$$

where $\overline{\mathcal{B}_q} := \{\beta \in [-\mathbf{1}, \mathbf{1}] \mid C\beta \leq d\} = \mathcal{B}_q \cap \langle C, d \rangle_H$ is the constrained unit-hypercube.

Compared to [33, Def. 3], we use inequality constraints instead of equality constraints for convenience. Both types of constraints are equivalent and can be translated by introducing slack variables. Moreover, the considered set-based operations, i.e., Minkowski sum (1) and affine map (2), are identical for zonotopes and constrained zonotope [33, Prop. 1]. Fig. 1 illustrates a constrained zonotope as a "shadow" of a constrained hypercube.

2.4 Formal Verification of Neural Networks

The output set of a neural network can be enclosed by conservatively propagating a zonotope through the layers of the neural network.

Proposition 1 (Set Propagation, [28, Sec. 2.4]). *Given a neural network $\Phi: \mathbb{R}^{n_0} \rightarrow \mathbb{R}^{n_\kappa}$ and an input set $\mathcal{X} \subset \mathbb{R}^{n_0}$, an enclosure $\mathcal{Y} = \text{enclose}(\Phi, \mathcal{X}) \subset \mathbb{R}^{n_\kappa}$ of the image $\mathcal{Y}^* := \Phi(\mathcal{X}) \subseteq \mathcal{Y}$ can be computed as*

$$\mathcal{H}_0 = \mathcal{X}, \quad \mathcal{H}_k = \text{enclose}(L_k, \mathcal{H}_{k-1}) \quad \text{for } k \in [\kappa], \quad \mathcal{Y} = \mathcal{H}_\kappa.$$

The operation $\text{enclose}(L_k, \mathcal{H}_{k-1})$ encloses the image of the k -th layer for the input set \mathcal{H}_{k-1} , i.e., $L_k(\mathcal{H}_{k-1}) \subseteq \text{enclose}(L_k, \mathcal{H}_{k-1})$ [28, Prop. 2.14]. If the k -th layer is linear, an affine map is applied (2): $\text{enclose}(L_k, \mathcal{H}_{k-1}) = W_k \mathcal{H}_{k-1} \oplus b_k$; otherwise, the activation function ϕ_k is enclosed with a linear function and corresponding approximation errors: $\text{enclose}(L_k, \mathcal{H}_{k-1}) = \text{diag}(m_k) \mathcal{H}_{k-1} \oplus [\underline{e}_k, \bar{e}_k]$, where $m_{k(i)}$ is the approximation slope and $[\underline{e}_{k(i)}, \bar{e}_{k(i)}]$ the approximation error of the i -th neuron, with $i \in [n_k]$ [26, Sec. IV].

2.5 Problem Statement

Given a neural network $\Phi: \mathbb{R}^{n_0} \rightarrow \mathbb{R}^{n_\kappa}$, an input set $\mathcal{X} \subset \mathbb{R}^{n_0}$, and unsafe set $\mathcal{U} \subset \mathbb{R}^{n_\kappa}$, our goal is to derive a fast and scalable algorithm that can either formally verify the safety of the neural network, i.e.,

$$\Phi(\mathcal{X}) \cap \mathcal{U} = \emptyset, \quad (3)$$

or find a counterexample, i.e.,

$$\exists x \in \mathcal{X}: \Phi(x) \in \mathcal{U}. \quad (4)$$

3 A Novel View on Zonotope Propagation

A zonotope is the "shadow" of a higher-dimensional hypercube (Fig. 1b). The propagation of a zonotope through the layers of a neural network transforms the projection of the hypercube, but the hypercube itself remains unchanged. Thus, all enclosed sets, i.e., the input and all hidden and output sets, are different "shadows" of the same hypercube. Therefore, the hypercube represents a latent space. Let us demonstrate this novel view by an example:

Example 1. *Fig. 2 illustrates the propagation of a two-dimensional input set \mathcal{X} (Fig. 2a) through a linear layer (Fig. 2b), i.e., $x \mapsto 2^{-1/2} \begin{bmatrix} 1 & -1 \\ 1 & 1 \end{bmatrix} x + \begin{bmatrix} 1 \\ 0 \end{bmatrix}$, and a nonlinear layer which applies the*

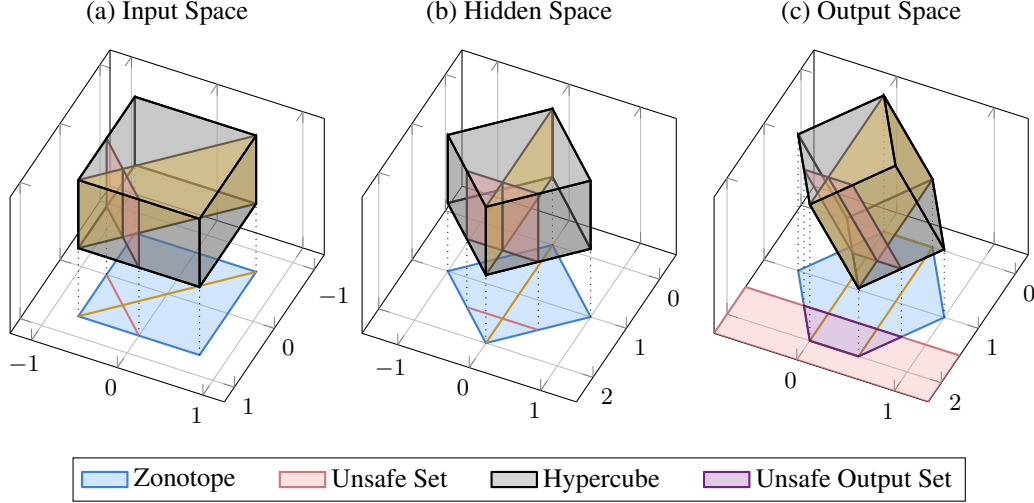


Figure 2: Illustrating the zonotope propagation through a linear layer and a nonlinear layer as the "shadows" of the same hypercube: (a) The input interval in the input space; (b) The output of the linear layer, which rotates and offsets the input set; (c) The output of the nonlinear layer tilts the hypercube to add the approximation errors. Using the hypercube, the unsafe set (\square) is transferred from the output space to the input space. Additionally, the hypercube is split along a hyperplane (\square) to exploit the piecewise linearity of the ReLU-activation function.

ReLU-activation function elementwise (Fig. 2c). Intuitively, the linear layer rotates the hypercube, and the nonlinear layer tilts it to compute the output set as its "shadow."

For input set $\mathcal{X} = \langle \mathbf{0}, 2^{-1/2} I_2 \rangle_Z$, the hidden set \mathcal{H}_1 and the \mathcal{Y} are computed using Prop. 1:

$$\begin{aligned} \mathcal{H}_1 &= 2^{-1/2} \begin{bmatrix} 1 & -1 \\ 1 & 1 \end{bmatrix} \mathcal{X} + \begin{bmatrix} 1 \\ 0 \end{bmatrix} = \left\langle \begin{bmatrix} 1 \\ 0 \end{bmatrix}, 1/2 \begin{bmatrix} 1 & -1 \\ 1 & 1 \end{bmatrix} \right\rangle_Z, \\ \mathcal{Y} &= \begin{bmatrix} 1 & 0 \\ 0 & 1/2 \end{bmatrix} \mathcal{H}_1 + \left[\begin{bmatrix} 0 \\ 0 \end{bmatrix}, \begin{bmatrix} 0 \\ 1/2 \end{bmatrix} \right] = \left\langle \begin{bmatrix} 1 \\ 1/4 \end{bmatrix}, 1/4 \begin{bmatrix} 2 & -2 & 0 \\ 1 & 1 & 1 \end{bmatrix} \right\rangle_Z. \end{aligned} \quad (5)$$

For each input $x \in \mathcal{X}$ and its corresponding output $y = \Phi(x) \in \mathcal{Y}$, we use the definition of a zonotope (Def. 2) to obtain $\beta \in [-1, 1]^3$ such that

$$x = \begin{bmatrix} 1/\sqrt{2} & 0 \\ 0 & 1/\sqrt{2} \end{bmatrix} \beta_{([2])}, \quad y = \begin{bmatrix} 1 \\ 1/4 \end{bmatrix} + \begin{bmatrix} 1/2 & -1/2 \\ 1/4 & 1/4 \end{bmatrix} \beta_{([2])} + \begin{bmatrix} 0 \\ 1/4 \end{bmatrix} \beta_{(3)}. \quad (6)$$

The input x and the output y are represented using the same factors $\beta_{([2])}$ with an additional factor $\beta_{(3)}$ for the approximation error. We can use an unsafe set $y_{(1)} \geq 3/2$ to formulate constraints (\square in Fig. 2) on the factors $\beta_{([2])}$ of the input:

$$y_{(1)} \geq 3/2 \stackrel{(6)}{\iff} 1 + [1/2 \quad -1/2] \beta_{([2])} + 0 \beta_{(3)} \geq 3/2 \iff [-1/2 \quad 1/2] \beta_{([2])} \leq -1/2. \quad (7)$$

Therefore, all unsafe inputs are enclosed by $\mathcal{X}|_{C \leq d}$, with $C = [-1/2 \quad 1/2]$ and $d = -1/2$. Analogously, we can split the set along $h_1 \leq 0 \iff [1/2 \quad 1/2] \beta_{([2])} \leq 0$, for $h_1 \in \mathcal{H}_1$, to exploit the piecewise linearity of the ReLU-activation function (\square in Fig. 2).

As example 1 demonstrates, we can transfer the specification from the output space to the input space to identify the subset of inputs that cause an intersection with a specification in the output space by exploiting the dependencies between the considered sets through the latent space. Prop. 2 formalizes an input refinement based on our observations.

Proposition 2 (Enclosing Unsafe Inputs). *Given are a neural network $\Phi: \mathbb{R}^{n_0} \rightarrow \mathbb{R}^{n_\kappa}$, an input set $\mathcal{X} = \langle c_x, G_x \rangle_Z \subset \mathbb{R}^{n_0}$ with $G_x \in \mathbb{R}^{n_0 \times q_0}$, and an unsafe set $\mathcal{U} = \langle A, b \rangle_H \subset \mathbb{R}^{n_\kappa}$. Let $\mathcal{Y} = \langle c_y, G_y \rangle_Z = \text{enclose}(\Phi, \mathcal{X})$ be an enclosure of the output set with $G_y \in \mathbb{R}^{n_\kappa \times q_\kappa}$. All unsafe inputs $\{x \in \mathcal{X} \mid \Phi(x) \in \mathcal{U}\}$ are enclosed by $\mathcal{X}|_{C \leq d}$, where $C := A G_{y(\cdot, [q_0])}$ and $d := b - A c_y + |A G_{y(\cdot, [q_\kappa] \setminus [q_0])}| \mathbf{1}$.*

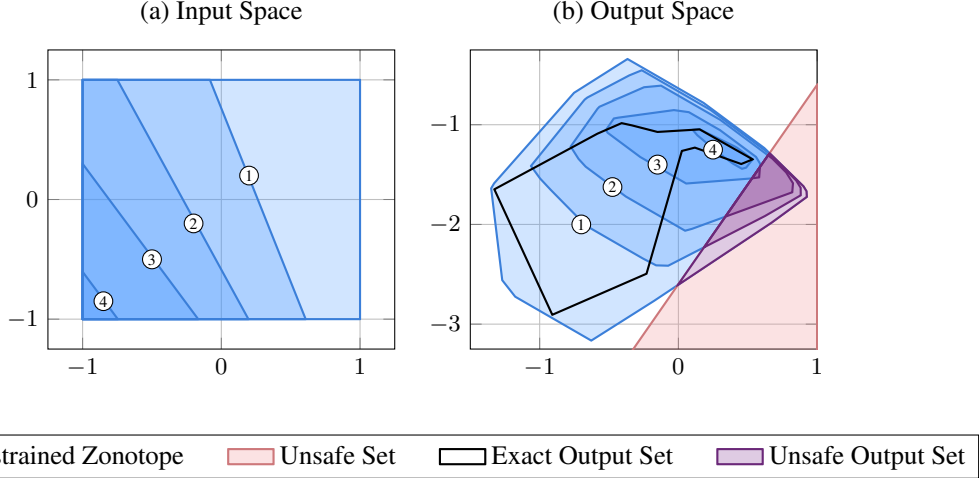


Figure 3: Illustration of an iterative refinement of the input set: The input set is iteratively refined (Prop. 2). After the fourth iteration, the intersection with the unsafe set is empty, and the neural network is verified.

Proof. See Appendix C.

We can use Prop. 2 to iteratively refine an input set to minimize the intersection of the computed output set and the specification. During each iteration, we transfer the specification from the output space to the input space to remove the parts of the input set which are provably safe. In Fig. 3, we iterate our input refinement until the problem is verified, i.e., the intersection of the output set and the unsafe set is empty.

4 Set-Based Falsification, Verification, and Input Refinement

For the fast and scalable verification of neural networks, we integrate our novel input refinement (Prop. 2) into a branch-and-bound procedure (Alg. 1). We perform the following computations in each iteration: (i) The output set of the current input set is enclosed (Prop. 1). (ii) The intersection with the unsafe set specification is checked (Sec. 4.1). (iii) If the intersection is non-empty, the verification is inconclusive, and falsification is attempted (Sec. 4.2). (iv) If no counterexample is found, the input set is refined and split (Sec. 4.3). The subsequent subsections describe the steps of Alg. 1 in detail.

4.1 Set-Based Verification

We compute the output set $\mathcal{Y} = \langle c_y, G_y \rangle_Z \subset \mathbb{R}^{n_\kappa}$ of the current input set using Prop. 1 and check if the intersection with the unsafe set $\mathcal{U} = \langle A, b \rangle_H \subset \mathbb{R}^{n_\kappa}$ with $A \in \mathbb{R}^{p \times n_\kappa}$ is empty [33, Prop. 2]:

$$\exists i \in [p]: A_{(i,\cdot)} c_y - |A_{(i,\cdot)} G_y| \mathbf{1} > b_{(i)} \implies \mathcal{Y} \cap \mathcal{U} = \emptyset. \quad (8)$$

4.2 Set-Based Falsification

If we cannot verify the current input set, we try to find a counterexample within it. Therefore, we utilize the latent space (Sec. 3) to transfer a boundary point of the output set along a normal vector of the unsafe set specification to the input space. For each normal vector of the unsafe set specification $A_{(i,\cdot)} \in \mathbb{R}^{n_\kappa}$, for $i \in [p]$, we compute a boundary point [3, Lemma 1]:

$$\tilde{\beta}_i = \text{sign}(A_{(i,\cdot)} G_y), \quad \tilde{y} = c_y + G_y \tilde{\beta}_i. \quad (9)$$

Finally, we check if the corresponding input $\tilde{x} = c_x + G_x \tilde{\beta}_{(q_0)} \in \mathcal{X}$ in the input set $\mathcal{X} = \langle c_x, G_x \rangle_Z$ with $G_x \in \mathbb{R}^{n_o \times q_o}$ is a counterexample, i.e., whether $\Phi(\tilde{x}) \in \mathcal{U}$.

Algorithm 1: Set-based verification algorithm. Input sets in a queue and we use the operations `initQueue`, `isNonEmpty`, `enqueue`, and `dequeue` from [23, Sec. 2.2.1]

Data: Neural network $\Phi: \mathbb{R}^{n_0} \rightarrow \mathbb{R}^{n_\kappa}$, input set $\mathcal{X} = \langle c_x, G_x \rangle_Z \subset \mathbb{R}^{n_0}$, unsafe set $\mathcal{U} = \langle A, b \rangle_H \subset \mathbb{R}^{n_\kappa}$

Result: Verification result: VERIFIED, FALSIFIED(\tilde{x}) with counterexample $\tilde{x} \in \mathcal{X}$

```

1 function verify( $\Phi, \mathcal{X}, \mathcal{U}$ )
2   Q  $\leftarrow$  initQueue(),  $i \leftarrow 1$                                 // Initialize queue & counter.
3   Q.enqueue( $\mathcal{X}$ )                                                // Add the initial input set.
4   while Q.isNonEmpty() do
5      $\mathcal{X}_i \leftarrow$  Q.dequeue()                                    // Get the next input set.
6      $\mathcal{Y}_i \leftarrow$  enclose( $\Phi, \mathcal{X}_i$ )                            // Enclose the output set (Prop. 1).
7     if  $\mathcal{Y}_i \cap \mathcal{U} = \emptyset$  then                               // 1. Verification (Sec. 4.1)
8       continue                                                // Verified input set.
9     else                                                        // 2. Falsification (Sec. 4.2)
10       $\tilde{x}_i \leftarrow$  Compute an adversarial input.                // (9)
11       $\tilde{y}_i \leftarrow \Phi(x)$                                        // Compute the adversarial output (Def. 1).
12      if  $\tilde{y}_i \in \mathcal{U}$  then
13        return FALSIFIED( $\tilde{x}_i$ )                                    // Found an unsafe input.
14      else                                                        // 3. Refinement & Splitting (Sec. 4.3)
15         $C, d \leftarrow$  Compute the constraints for the input set. // Prop. 2
16         $\mathcal{X}_i|_{C_1 \leq d_1}, \dots, \mathcal{X}_i|_{C_\xi \leq d_\xi} \leftarrow$  Refine and split the input set. // Prop. 2, [33, Prop. 3]
17        Q.enqueue( $\mathcal{X}_i|_{C_1 \leq d_1}, \dots, \mathcal{X}_i|_{C_\xi \leq d_\xi}$ ) // Add new sets to the queue.
18         $i \leftarrow i + 1$                                        // Increment the counter.
19      end
20    end
21  end
22  return VERIFIED                                             // Queue is empty; verified all input sets.

```

4.3 Input Set Refinement and Constraint-Based Input Splitting

Finally, if we cannot verify the input set nor find a counterexample, we refine the input set using Prop. 2.

Corollary 1. *Given a neural network $\Phi: \mathbb{R}^{n_0} \rightarrow \mathbb{R}^{n_\kappa}$, an input set $\mathcal{X} \subset \mathbb{R}^{n_0}$, and unsafe set $\mathcal{U} = \langle A, b \rangle_H \subset \mathbb{R}^{n_\kappa}$, the refinement of the input set (Prop. 2) can be used for verification and falsification*

$$\begin{aligned} \Phi(\mathcal{X}|_{C \leq d}) \cap \mathcal{U} = \emptyset &\iff \Phi(\mathcal{X}) \cap \mathcal{U} = \emptyset, \\ \exists x \in \mathcal{X}|_{C \leq d}: \Phi(x) \in \mathcal{U} &\iff \exists x \in \mathcal{X}: \Phi(x) \in \mathcal{U}. \end{aligned}$$

Proof. See Appendix C.

Moreover, we reduce the conservatism of the zonotope propagation by splitting the refined input set through additional constraints of the hypercube [33, Prop. 3]; e.g., we can formulate constraints that exploit the piecewise linearity of the ReLU-activation function (■ in Fig. 2).

5 Evaluation

We have implemented our verification algorithm in MATLAB. To make our evaluation as transparent and reproducible as possible, we compare the results of our tool on benchmarks from the neural network verification competition 2024 (VNN-COMP'24) [8] with the top-5 tools of last year's competition: α - β -CROWN [36], NeuralSAT [12], PyRat [29], Marabou [38], and nnenum [4].

Tab. 1 presents the results for 7 competitive and standardized benchmarks of the VNN-COMP'24 [8]. Please see Appendix A for details. Across all benchmarks, our verification algorithm achieves competitive performance, even matching the top performance in three benchmarks. These results would place our tool in the top 5 of the competition.

Table 1: Main Results [%Solved (#Verified / #Falsified)].

Tool	Benchmark						
	acasxu	collins -rul-cnn	cora	dist-shift	metaroom	safenlp	tllverify -bench
Ours	98.9% (138 / 46)	100.0% (30 / 32)	80.0% (18 / 126)	98.6% (63 / 8)	96.0% (89 / 7)	84.3% (289 / 621)	100.0% (15 / 17)
<i>Results from VNN-COMP'24 [8]</i>							
α - β -CROWN	100.0% (139 / 47)	100.0% (30 / 32)	87.8% (24 / 134)	98.6% (63 / 8)	98.0% (91 / 7)	100.0% (421 / 659)	100.0% (15 / 17)
NeuralSAT	98.9% (138 / 46)	100.0% (30 / 32)	87.2% (23 / 134)	98.6% (63 / 8)	98.0% (91 / 7)	90.5% (327 / 650)	100.0% (15 / 17)
PyRAT	98.9% (137 / 47)	93.5% (30 / 28)	83.3% (22 / 128)	98.6% (63 / 8)	97.0% (91 / 6)	79.9% (277 / 586)	100.0% (15 / 17)
Marabou	96.2% (134 / 45)	100.0% (30 / 32)	86.7% (22 / 134)	95.8% (62 / 7)	53.0% (46 / 7)	62.5% (300 / 375)	93.8% (13 / 17)
nnenum	99.5% (139 / 46)	100.0% (30 / 32)	14.4 (20 / 6)	– (– / –)	46.0% (44 / 2)	89.2% (321 / 642)	56.2% (2 / 16)

Table 2: Ablation studies.

(a) Comparing Refinement [avg. #Sub-problems].

Refinement	acasxu	
	prop_1	prop_3
none	1073.4	24785.6
network-wise	406.9	1983.0
layer-wise	406.1	1024.3

(b) GPU Acceleration and Batch Size [avg. Time (%Solved)].

Method	Batch size	acasxu	
		prop_1	prop_3
CPU	1	11.6s (97.8%)	6.5s (95.6%)
	128	3.9s (100.0%)	4.8s (97.8%)
	1024	5.1s (100.0%)	5.7s (97.8%)
GPU	1	37.5s (88.9%)	12.4s (93.3%)
	128	3.0s (100.0%)	4.4s (97.8%)
	1024	1.9s (100.0%)	1.8s (100.0%)

5.1 Ablation Studies

We run extensive ablation studies to justify the different design choices of our algorithm.

Falsification Method We justify our set-based adversarial attack (Sec. 4.2) by comparing it with using the center of the output enclosure for falsification and the fast-gradient-sign method (FGSM) [17] on the `safenlp` benchmark. Tab. 3 presents the results that show that our set-based adversarial attack performs best.

Input Refinement We evaluate the improvement through our input refinement. Therefore, we compare doing no refinement (none) with network-wise refinement and layer-wise refinement. The network-wise refinement directly transfers the specification from the output space to the input space. In contrast, the layer-wise refinement incrementally transfers the specification through the layers, which has the advantage that only subsequent approximation errors need to be considered. Our refinement significantly reduces the number of subproblems in all cases. The layer-wise refinement performs slightly better than the network-wise refinement (Tab. 2a).

GPU Acceleration and Batch Size We demonstrate the efficacy and speed up of the GPU acceleration by comparing the results of the `acasxu` benchmark computed on a CPU and with different batch sizes (Tab. 2b).

Table 3: Comparing Falsification Methods [#Falsified (%Solved)].

Falsification	safenlp
center	176 (16.3%)
FGSM	274 (25.4%)
Set-based	621 (57.5%)

6 Related Work

Neural Network Verification and Adversarial Attacks Most algorithms for neural network verification either (i) formulate an optimization or constraint satisfaction problem and apply an off-the-shelf solver, e.g., satisfiability modulo theories [22, 12, 38] or (mixed-integer) linear programming [35, 30], or (ii) use abstract interpretation or reachability analysis to enclose the intersection of the specification with the output of the neural network [15, 37, 34, 36, 25, 28, 29].

The most common abstract domains or set representations are intervals [15], zonotopes [15], or polytopes [30, 41, 34], that use linear relaxations of activation functions for the propagation. More complex set representations can enclose the output set more tightly, e.g., polynomial zonotopes [25], hybrid zonotopes [31], star sets [4]; however, due to higher computational cost, these approaches do not scale to large neural networks. The results of multiple abstract domains can be combined to obtain a tighter enclosure [29]. A popular abstract domain, DeepPoly/CROWN [34, 41], uses bounded polytopes, which are represented as the intersection of linear bounds and intervals. Further, gradient-based optimization can be applied to bounding parameters to tighten the computed enclosure [36].

If formal verification is computationally infeasible, an alternative is to falsify neural networks using adversarial attacks. Often, gradient-based attacks are fast and effective at finding adversarial perturbations [17, 27]. Further, stronger adversarial examples can be computed with optimization-based approaches [10]. Our set-based falsification does not require the gradient of the neural network while being faster to compute than an optimization problem.

Iterative Neural Network Refinement There are different iterative refinement approaches, e.g., refining bounds using (mixed-integer) linear programs [37, 35], counterexample guided abstraction refinement [38], and refining the hyperparameters of output set enclosure [39, 28]. Our novel specification-driven input refinement iteratively encloses the set of inputs that cause an intersection with an unsafe set in the output space. Therefore, our refinement does not require tuning hyperparameters or solving expensive (mixed-integer) linear programs. The refinement procedure uses dependencies between propagated zonotopes, which can be used to simplify computations for reachability analysis or identify falsifying states [24].

Branch-and-Bound Algorithms and Splitting Heuristics For large neural networks, most verification approaches are too conservative. Therefore, in practice, most verification approaches use a branch-and-bound procedure that recursively splits the verification problem into smaller subproblems that are easier to solve [7, 8], e.g., by exploiting the piece-wise linearity of the ReLU-activation function. There are various approaches and heuristics for splitting a verification problem, e.g., largest radius, largest approximation error and its effect on the output constraints [18], gradient or sensitivity-based heuristics to estimate the impact of a neuron on the output [5, 13, 28], magnitude of the coefficient of linear relaxation [13], largest unstable neuron in the first undecidable layer [40], multi-neuron constraints [14], least unstable neuron [12].

7 Conclusion

In this paper, we construct a novel latent space for an iterative refinement procedure to speed up the formal verification of neural networks. The latent space is constructed from the propagation of projection-based set representations, e.g., zonotopes, through the layers of a neural network. Our procedure iteratively refines an enclosure of the set of unsafe inputs by using the latent space to transfer the specification from the output space to the input space. We integrate our refinement procedure in a branch-and-bound neural network verification algorithm and in an extensive evaluation we show a significantly reduction of the number of recursive splits required verification. Moreover, we show that our algorithm achieves competitive performance compared to the top-5 tools of the last neural network verification competition. In summary, our novel latent space presents a promising new direction for the formal verification of neural networks.

Acknowledgements

This work was partially supported by the project SPP-2422 (No. 500936349) and the project FAI (No. 286525601), both funded by the German Research Foundation (Deutsche Forschungsgemeinschaft,

DFG). We also want to thank our colleague Roland Stolz from our research group for their revisions of the manuscript.

References

- [1] Matthias Althoff. “An introduction to CORA 2015”. In: *ARCH Workshop*. 2015, pp. 120–151.
- [2] Matthias Althoff. “Reachability analysis and its application to the safety assessment of autonomous cars”. PhD thesis. Technische Universität München, 2010.
- [3] Matthias Althoff and Goran Frehse. “Combining zonotopes and support functions for efficient reachability analysis of linear systems”. In: *CDC*. 2016, pp. 7439–7446.
- [4] Stanley Bak. “nenum: Verification of relu neural networks with optimized abstraction refinement”. In: *NASA formal methods symposium*. 2021, pp. 19–36.
- [5] Mislav Balunovic et al. “Certifying Geometric Robustness of Neural Networks”. In: *NeurIPS*. Vol. 32. 2019.
- [6] Christopher Bishop. *Pattern recognition and machine learning*. Springer New York, NY, 2006.
- [7] Christopher Brix et al. “First three years of the international verification of neural networks competition (VNN-COMP)”. In: *STTT* 25.3 (2023), pp. 329–339.
- [8] Christopher Brix et al. “The Fifth International Verification of Neural Networks Competition (VNN-COMP 2024): Summary and Results”. In: *arXiv preprint arXiv:2412.19985* (2024).
- [9] Rudy Bunel et al. “A Unified View of Piecewise Linear Neural Network Verification”. In: *NeurIPS*. Vol. 31. 2018.
- [10] Nicholas Carlini and David Wagner. “Towards Evaluating the Robustness of Neural Networks”. In: *IEEE SSP*. 2017, pp. 39–57.
- [11] Pranav Singh Chib and Pravendra Singh. “Recent advancements in end-to-end autonomous driving using deep learning: A survey”. In: *IEEE T-IV* 9.1 (2023), pp. 103–118.
- [12] Hai Duong, ThanhVu Nguyen, and Matthew Dwyer. “A DPLL (T) framework for verifying deep neural networks”. In: *arXiv preprint arXiv:2307.10266* (2023).
- [13] Serge Durand et al. “ReCIPH: Relational coefficients for input partitioning heuristic”. In: *WFVML*. 2022.
- [14] Claudio Ferrari et al. “Complete Verification via Multi-Neuron Relaxation Guided Branch-and-Bound”. In: *ICLR*. 2022.
- [15] Timon Gehr et al. “AI2: Safety and Robustness Certification of Neural Networks with Abstract Interpretation”. In: *IEEE SSP*. 2018, pp. 3–18.
- [16] Antoine Girard. “Reachability of Uncertain Linear Systems Using Zonotopes”. In: *HSCC*. 2005, pp. 291–305.
- [17] Ian Goodfellow, Jonathon Shlens, and Christian Szegedy. “Explaining and Harnessing Adversarial Examples”. In: *ICLR*. 2015.
- [18] Patrick Henriksen and Alessio Lomuscio. “DEEPSPLIT: An Efficient Splitting Method for Neural Network Verification via Indirect Effect Analysis”. In: *IJCAI*. 2021, pp. 2549–2555.
- [19] Ahmed Irfan et al. “Towards Verification of Neural Networks for Small Unmanned Aircraft Collision Avoidance”. In: *DASC*. 2020, pp. 1–10.
- [20] Radoslav Ivanov et al. “Verisig: verifying safety properties of hybrid systems with neural network controllers”. In: *HSCC*. 2019, pp. 169–178.
- [21] John Jumper et al. “Highly accurate protein structure prediction with AlphaFold”. In: *Nature* 596.7873 (2021), pp. 583–589.
- [22] Guy Katz et al. “Reluplex: An Efficient SMT Solver for Verifying Deep Neural Networks”. In: *CAV*. 2017, pp. 97–117.
- [23] Donald Knuth. *The Art of Computer Programming*. Vol. 1: Fundamental Algorithms. Addison-Wesley, 1997.
- [24] Niklas Kochdumper, Bastian Schürmann, and Matthias Althoff. “Utilizing dependencies to obtain subsets of reachable sets”. In: *HSCC*. 2020.
- [25] Niklas Kochdumper et al. “Open- and Closed-Loop Neural Network Verification Using Polynomial Zonotopes”. In: *NASA Formal Methods*. 2023, pp. 16–36.
- [26] Lukas Koller, Tobias Ladner, and Matthias Althoff. “Set-Based Training for Neural Network Verification”. In: *arXiv preprint arXiv:2401.14961* (2025).

- [27] Alexey Kurakin, Ian Goodfellow, and Samy Bengio. “Adversarial Machine Learning at Scale”. In: *ICLR*. 2017.
- [28] Tobias Ladner and Matthias Althoff. “Automatic Abstraction Refinement in Neural Network Verification Using Sensitivity Analysis”. In: *HSCC*. 2023, pp. 1–13.
- [29] Augustin Lemesle, Julien Lehmann, and Tristan Le Gall. “Neural Network Verification with PyRAT”. In: *arXiv preprint arXiv:2410.23903* (2024).
- [30] Mark Niklas Müller et al. “PRIMA: general and precise neural network certification via scalable convex hull approximations”. In: *PACMPL* 6.POPL (2022).
- [31] Joshua Ortiz et al. “Hybrid zonotopes exactly represent ReLU neural networks”. In: *CDC*. 2023, pp. 5351–5357.
- [32] Alexander Schrijver. *Theory of linear and integer programming*. John Wiley & Sons, 1998.
- [33] Joseph Scott et al. “Constrained zonotopes: A new tool for set-based estimation and fault detection”. In: *Automatica* 69 (2016), pp. 126–136.
- [34] Gagandeep Singh et al. “An abstract domain for certifying neural networks”. In: *PACMPL* 3.POPL (2019).
- [35] Gagandeep Singh et al. “Boosting Robustness Certification of Neural Networks”. In: *ICLR*. 2019.
- [36] Shiqi Wang et al. “Beta-crown: Efficient bound propagation with per-neuron split constraints for neural network robustness verification”. In: *NeurIPS* 34 (2021), pp. 29909–29921.
- [37] Shiqi Wang et al. “Efficient formal safety analysis of neural networks”. In: *NeurIPS*. 2018, pp. 6369–6379.
- [38] Haoze Wu et al. “Marabou 2.0: a versatile formal analyzer of neural networks”. In: *CAV*. 2024, pp. 249–264.
- [39] Kaidi Xu et al. “Fast and Complete: Enabling Complete Neural Network Verification with Rapid and Massively Parallel Incomplete Verifiers”. In: *ICLR*. 2021.
- [40] Banghu Yin et al. “Efficient Complete Verification of Neural Networks via Layerwise Splitting and Refinement”. In: *IEEE TCAD* 41.11 (2022), pp. 3898–3909.
- [41] Huan Zhang et al. “Efficient neural network robustness certification with general activation functions”. In: *NeurIPS* 31 (2018).
- [42] Zhengxia Zou et al. “Object detection in 20 years: A survey”. In: *Proc. IEEE* 111.3 (2023), pp. 257–276.

A Appendix – Evaluation Details

For the evaluation, we implement our verification algorithm in MATLAB using the CORA [1] toolbox. The experiments are run on a server with 2×AMD EPYC 7763 (64 cores/128 threads), 2TB RAM, and a NVIDIA A100 40GB GPU.

The selected benchmarks are taken from the VNN-COMP’24 [8]: `acasxu` a standard benchmark used by many prior works containing neural networks for airborne collision detection; `collins-rul-cnn` containing neural networks for condition-based maintenance; `cora` and `metaroom` containing neural networks for high-dimensional image classification; `dist-shift` containing neural networks for distribution shift detection; `safeNLP` containing neural networks for sentence classification; `t11verifybench` containing two-level lattice neural networks.

To produce the main results (Tab. 1) we use the following parameters: batch size of 1024 (is automatically halved if there is out of memory error); GPU acceleration is enabled; in each iteration the largest-most sensitive input dimension is split along the middle; the zonotope propagation uses the same enclosure as [26].

B Appendix – Implementation Tricks

We efficiently implement our algorithm with only matrix operations to take full advantage of GPU acceleration. Further, to make our algorithm practical, we reduce the memory footprint by only storing the bounds of the constrained zonotopes in the queue. We use zonotopes for the set propagation (line 6). However, we compute the bounds of a constrained zonotope before an enqueue operation.

Computing the bounds of constrained zonotopes requires solving two linear programs for each dimension, which limits GPU acceleration. Hence, we avoid solving linear programs by efficiently approximating the bounds of a constrained zonotope by approximating the bounds of the constrained hypercube (Prop. 3). The approximation is inspired by the Fourier-Motzkin elimination [32, Sec. 12.2].

To avoid clutter, we introduce further notation: For a matrix $A \in \mathbb{R}^{n \times m}$, we denote the matrix with all non-positive entries set to zero with $A^+ \in \mathbb{R}_{\geq 0}$, i.e., $A^+ = 1/2(A + |A|)$; the matrix $A^- \in \mathbb{R}_{\geq 0}$ is defined analogously.

Proposition 3 (Bounds of Bounded Polytope). *A constrained hypercube $\mathcal{P} = \langle C, d \rangle_H \cap [\underline{\beta}_0, \bar{\beta}_0] \subset \mathbb{R}^q$ with $C \in \mathbb{R}^{p \times q}$ and $d \in \mathbb{R}^p$ is enclosed by $[\underline{\beta}, \bar{\beta}]$, i.e., $\mathcal{P} \subseteq [\underline{\beta}, \bar{\beta}]$. For each dimension $j \in [q]$, let $\Sigma_{\setminus\{j\}} := I_q - \mathbf{e}_j \mathbf{e}_j^\top$, and for each $i \in [p]$, let $\underline{C}_{(i,j)} := (d_{(i)} - C_{(i,\cdot)}^+ \Sigma_{\setminus\{j\}} \underline{\beta}_0 - C_{(i,\cdot)}^- \Sigma_{\setminus\{j\}} \bar{\beta}_0) / C_{(i,j)}$. The bounds of \mathcal{P} are computed by*

$$\begin{aligned} \underline{\beta}_{(j)} &= \max \{ \underline{C}_{(i,j)} \mid i \in [p]: C_{(i,j)} < 0 \} \cup \{ \underline{\beta}_{0(j)} \}, \\ \bar{\beta}_{(j)} &= \min \{ \underline{C}_{(i,j)} \mid i \in [p]: C_{(i,j)} > 0 \} \cup \{ \bar{\beta}_{0(j)} \}. \end{aligned}$$

Proof. We fix a point $\beta \in \mathcal{P}$ and indices $i \in [p]$ and $j \in [q]$ and show that $\beta \in [\underline{\beta}, \bar{\beta}]$. From the definition of a polytope, it holds that: $C_{(i,\cdot)} \beta \leq d_{(i)}$. By rearranging the terms, we obtain

$$C_{(i,\cdot)} \beta \leq d_{(i)} \iff C_{(i,j)} \beta_{(j)} \leq d_{(i)} - \sum_{k \in [q] \setminus \{j\}} C_{(i,k)} \beta_{(k)} = d_{(i)} - C_{(i,\cdot)} \Sigma_{\setminus\{j\}} \beta.$$

We split cases on the sign of $C_{(i,j)}$:

Case 1 ($C_{(i,j)} < 0$). We obtain a lower bound for $\beta_{(j)}$:

$$\frac{d_{(i)} - C_{(i,\cdot)} \Sigma_{\setminus\{j\}} \beta}{C_{(i,j)}} \leq \beta_{(j)}.$$

Using the initial bounds, i.e., $\underline{\beta}_{0(j)} \leq \beta_{(j)} \leq \bar{\beta}_{0(j)}$, we can approximate the bounds of $\beta_{(j)}$:

$$\begin{aligned} \beta_{(j)} &\stackrel{(C_{(i,j)} < 0)}{\geq} \frac{d_{(i)} - C_{(i,\cdot)} \Sigma_{\setminus\{j\}} \beta}{C_{(i,j)}} \geq \min_{\tilde{\beta} \in \mathcal{P}} \frac{d_{(i)} - C_{(i,\cdot)} \Sigma_{\setminus\{j\}} \tilde{\beta}}{C_{(i,j)}} \geq \min_{\tilde{\beta} \in [\underline{\beta}_0, \bar{\beta}_0]} \frac{d_{(i)} - C_{(i,\cdot)} \Sigma_{\setminus\{j\}} \tilde{\beta}}{C_{(i,j)}} \\ &= \frac{d_{(i)} - \min_{\tilde{\beta} \in [\underline{\beta}_0, \bar{\beta}_0]} C_{(i,\cdot)} \Sigma_{\setminus\{j\}} \tilde{\beta}}{C_{(i,j)}} = \frac{d_{(i)} - C_{(i,\cdot)}^+ \Sigma_{\setminus\{j\}} \underline{\beta}_0 - C_{(i,\cdot)}^- \Sigma_{\setminus\{j\}} \bar{\beta}_0}{C_{(i,j)}} = \underline{C}_{(i,j)}. \end{aligned}$$

Case 2 ($C_{(i,j)} > 0$). We obtain an upper bound for $\beta_{(j)}$:

$$\beta_{(j)} \leq \frac{d_{(i)} - C_{(i,\cdot)} \Sigma_{\setminus\{j\}} \beta}{C_{(i,j)}}.$$

Using the initial bounds, i.e., $\underline{\beta}_{0(j)} \leq \beta_{(j)} \leq \bar{\beta}_{0(j)}$, we can approximate the bounds of $\beta_{(j)}$:

$$\begin{aligned} \beta_{(j)} &\stackrel{(C_{(i,j)} > 0)}{\leq} \frac{d_{(i)} - C_{(i,\cdot)} \Sigma_{\setminus\{j\}} \beta}{C_{(i,j)}} \leq \max_{\tilde{\beta} \in \mathcal{P}} \frac{d_{(i)} - C_{(i,\cdot)} \Sigma_{\setminus\{j\}} \tilde{\beta}}{C_{(i,j)}} \leq \max_{\tilde{\beta} \in [\underline{\beta}_0, \bar{\beta}_0]} \frac{d_{(i)} - C_{(i,\cdot)} \Sigma_{\setminus\{j\}} \tilde{\beta}}{C_{(i,j)}} \\ &= \frac{d_{(i)} - \min_{\tilde{\beta} \in [\underline{\beta}_0, \bar{\beta}_0]} C_{(i,\cdot)} \Sigma_{\setminus\{j\}} \tilde{\beta}}{C_{(i,j)}} = \frac{d_{(i)} - C_{(i,\cdot)}^+ \Sigma_{\setminus\{j\}} \underline{\beta}_0 - C_{(i,\cdot)}^- \Sigma_{\setminus\{j\}} \bar{\beta}_0}{C_{(i,j)}} = \underline{C}_{(i,j)}. \end{aligned}$$

Each row i of the constraint matrix C generates an inequality for each dimension j of β . Thus, with $\beta \in [\underline{\beta}_0, \bar{\beta}_0]$, we set $\underline{\beta}_{(j)}$ to maximum lower bound and $\bar{\beta}_{(j)}$ to minimum lower bound. \square

Note that Prop. 3 can be iterated: For $\mathcal{P} = \langle C, d \rangle_H \cap [\underline{\beta}_0, \bar{\beta}_0]$ with bounds $[\underline{\beta}, \bar{\beta}]$, it holds that $\mathcal{P} = \langle C, d \rangle_H \cap [\underline{\beta}, \bar{\beta}]$; thus, Prop. 3 can be applied again to obtain potentially smaller bounds.

The bounds of a constrained zonotope $\mathcal{Z}|_{C \leq d} \subset \mathbb{R}^n$ with $\mathcal{Z} = \langle c, G \rangle_Z$ can be approximated by applying an affine map to the bounds $[\underline{\beta}, \overline{\beta}] \subseteq \overline{\mathcal{B}}_q$ of its constrained hypercube:

$$\mathcal{Z}|_{C \leq d} \subseteq c \oplus G^- [\underline{\beta}, \overline{\beta}] \oplus G^+ [\underline{\beta}, \overline{\beta}]. \quad (10)$$

C Appendix – Proofs

Proposition 2. *Given are a neural network $\Phi: \mathbb{R}^{n_0} \rightarrow \mathbb{R}^{n_\kappa}$, an input set $\mathcal{X} = \langle c_x, G_x \rangle_Z \subset \mathbb{R}^{n_0}$ with $G_x \in \mathbb{R}^{n_0 \times q_0}$, and an unsafe set $\mathcal{U} = \langle A, b \rangle_H \subset \mathbb{R}^{n_\kappa}$. Let $\mathcal{Y} = \langle c_y, G_y \rangle_Z = \text{enclose}(\Phi, \mathcal{X})$ be an enclosure of the output set with $G_y \in \mathbb{R}^{n_\kappa \times q_\kappa}$. All unsafe inputs $\{x \in \mathcal{X} \mid \Phi(x) \in \mathcal{U}\}$ are enclosed by $\mathcal{X}|_{C \leq d}$, where $C := A G_{y(\cdot, [q_0])}$ and $d := b - A c_y + |A G_{y(\cdot, [q_\kappa] \setminus [q_0])}| \mathbf{1}$.*

Proof. We fix an unsafe input $x \in \{x \in \mathcal{X} \mid \Phi(x) \in \mathcal{U}\}$. Let $y = \Phi(x)$ be its corresponding output. We use the definition of the unsafe set \mathcal{U} and the definition of a zonotope, i.e., there are factors $\beta \in \mathcal{B}_{q_\kappa}$ s.t.

$$y = c_y + G_y \beta. \quad (11)$$

For an unsafe output we have the following inequality:

$$y \in \mathcal{U} \stackrel{(11)}{\iff} A(c_y + G_y \beta) \leq b \iff A G_y \beta \leq b - A c_y.$$

Please note that the first q_0 factors of the output y are the factors of the input x , i.e., $x = c_x + G_x \beta_{([q_0])}$. Our goal is to constrain the factors $\beta_{([q_0])}$. Therefore, we rearrange the terms

$$\begin{aligned} A G_y \beta \leq b - A c_y &\iff A G_{y(\cdot, [q_0])} \beta_{([q_0])} + A G_{y(\cdot, [q_\kappa] \setminus [q_0])} \beta_{([q_\kappa] \setminus [q_0])} \leq b - A c_y \\ &\iff C \beta_{([q_0])} \leq b - (A c_y + A G_{y(\cdot, [q_\kappa] \setminus [q_0])} \beta_{([q_\kappa] \setminus [q_0])}). \end{aligned}$$

We bound the right hand side to get to obtain constraints $C \beta_{([q_0])} \leq d$ on the factors of x :

$$C \beta_{([q_0])} \leq b - (A c_y + A G_{y(\cdot, [q_\kappa] \setminus [q_0])} \beta_{([q_\kappa] \setminus [q_0])}) \leq b - A c_y + |A G_{y(\cdot, [q_\kappa] \setminus [q_0])}| \mathbf{1} = d.$$

Thus, we conclude that the input x is contained in the constrained input set \mathcal{X} :

$$x \in \mathcal{X}|_{C \leq d}. \quad \square$$

Corollary 1. *Given a neural network $\Phi: \mathbb{R}^{n_0} \rightarrow \mathbb{R}^{n_\kappa}$, an input set $\mathcal{X} \subset \mathbb{R}^{n_0}$, and unsafe set $\mathcal{U} = \langle A, b \rangle_H \subset \mathbb{R}^{n_\kappa}$, the refinement of the input set (Prop. 2) can be used for verification and falsification*

$$\begin{aligned} \Phi(\mathcal{X}|_{C \leq d}) \cap \mathcal{U} = \emptyset &\iff \Phi(\mathcal{X}) \cap \mathcal{U} = \emptyset, \\ \exists x \in \mathcal{X}|_{C \leq d}: \Phi(x) \in \mathcal{U} &\iff \exists x \in \mathcal{X}: \Phi(x) \in \mathcal{U}. \end{aligned}$$

Proof. With Prop. 2 we obtain $\mathcal{X} \setminus \mathcal{X}|_{C \leq d} \subseteq \{x \in \mathcal{X} \mid \Phi(x) \notin \mathcal{U}\}$, and therefore, we have $\Phi(\mathcal{X} \setminus \mathcal{X}|_{C \leq d}) \cap \mathcal{U} = \emptyset$ and $\neg(\exists x \in \mathcal{X} \setminus \mathcal{X}|_{C \leq d}: \Phi(x) \in \mathcal{U})$. Thus,

$$\begin{aligned} \Phi(\mathcal{X}|_{C \leq d}) \cap \mathcal{U} = \emptyset &\iff \Phi(\mathcal{X}|_{C \leq d}) \cap \mathcal{U} = \emptyset \wedge \Phi(\mathcal{X} \setminus \mathcal{X}|_{C \leq d}) \cap \mathcal{U} = \emptyset \\ &\iff (\Phi(\mathcal{X}|_{C \leq d}) \cup \Phi(\mathcal{X} \setminus \mathcal{X}|_{C \leq d})) \cap \mathcal{U} = \emptyset \\ &\iff \Phi(\mathcal{X}) \cap \mathcal{U} = \emptyset, \end{aligned}$$

$$\begin{aligned} \exists x \in \mathcal{X}|_{C \leq d}: \Phi(x) \in \mathcal{U} &\iff \exists x \in \mathcal{X}|_{C \leq d}: \Phi(x) \in \mathcal{U} \vee \exists x \in \mathcal{X} \setminus \mathcal{X}|_{C \leq d}: \Phi(x) \in \mathcal{U} \\ &\iff \exists x \in (\mathcal{X}|_{C \leq d} \cup \mathcal{X} \setminus \mathcal{X}|_{C \leq d}): \Phi(x) \in \mathcal{U} \\ &\iff \exists x \in \mathcal{X}: \Phi(x) \in \mathcal{U}. \quad \square \end{aligned}$$